Korean Chem. Eng. Res., 61(2), 312-321 (2023)
https://doi.org/10.9713/kcer.2023.61.2.312
PISSN 0304-128X, EISSN 2233-9558

Effects of Geometry and Operating Fluid on the Expansion Behavior of Liquid-Solid Fluidized Beds

Mohsen Mozafari-Shamsi*,†, Alireza Malooze, Mohammad Sefid**, Mostafa Soroor*** and Ehsan Mehrabi Gohari******

*Department of Engineering, Meybod University, 8961699557, Meybod, Iran
**Department of Mechanical Engineering, Yazd University, 8915818411, Yazd, Iran
***Department of Mechanical Engineering, Tarbiat Modares University, 14115111, Tehran, Iran
****Department of Mechanical Engineering, Payam-e-Noor University, Tehran, Iran
(Received 8 October 2022; Received in revised from 3 March 2023; Accepted 8 March 2023)

Abstract – Fluidized beds have been widely used in industrial applications, which in most of them, the operating fluid is non-Newtonian. In this study, the combination of the lattice Boltzmann method (LBM) and the smoothed profile method has been developed for non-Newtonian power-law fluids. The validation of the obtained model were investigated by experimental correlations. This model has been used for numerical studying of changing the operating fluid and geometrical parameters on the expansion behavior in liquid-solid beds with both Newtonian and non-Newtonian fluids. Investigations were performed for seven different geometries, one Newtonian, and two non-Newtonian fluids. The power-law index was in the range of 0.8 to 1, and the results for the Newtonian fluidized beds show more porosity than the non-Newtonian ones. Furthermore, increasing the power-law index resulted in enhancing the bed porosity. On the other hand, bed porosity was decreased by increasing the initial bed height and the density of the solid particles. Finally, the porosity ratio in the bed was decreased by increasing the solid particle diameter.

Key words: Liquid-solid fluidized bed, Lattice boltzmann, Smoothed profile, Power-law non-Newtonian fluid, Fluidized bed porosity

1. Introduction

Fluidized beds (and fluidization process) is a common operation in industrial processes for separation, increasing mass transfer rate, heat transfer, moisture absorption, and catalytic processes in chemical reactions. A fluidized bed is suspended by passing the operating fluid through the solid particles. In these beds, the vertical flow of fluid flows through the bed from the bottom upwards. The lift force on the solid particles increases with increasing inlet fluid velocity and, eventually, the lift force equals the weight of the particle. As the inlet fluid velocity increases, the bed begins to expand. In this case, the behavior of solid particles in the bed is very similar to the behavior of fluids, which is known as fluidization [1].

Fluidized beds have been used in many industries, including petroleum, petrochemical, biochemical, metallurgical, and even pharmaceutical and food industries [2], which in most applications, the operating fluid on the beds has non-Newtonian behavior [3]. Researchers have been working on understanding and clarifying the physics of these beds with non-Newtonian fluid as the operating fluid. In this regard, Yu et al. [4], Mishra et al. [5], Brea et al. [6], Kumar, and Upadhyay [7], and Kawase and Ulbrecht [8] all experimentally studied the liquid-solid non-Newtonian fluidized beds. They all used piezoplastic fluid in their study and presented the bed expansion characteristic as a function of fluid rheology.

Benedict et al. [9] experimentally investigated the inverse liquid-solid non-Newtonian fluidized bed. In this study, solid particles were 6mm-diameter, low-density polyethylene and polypropylene, and non-Newtonian fluid was 0.1% carboxyl methylcellulose (CMC) water solution. Benedict et al. observed that as the solution density increased, the minimum fluidization rate decreased. He presented an empirical relationship to estimate bed height in full fluidization. Lakshmi et al. [10] also performed a similar experimental investigation in a similar bed with low-density polyethylene particles and polypropylene with a range of diameter of 4 to 8 mm and different concentrations of CMC solution. He presented two experimental relationships to estimate the coefficient of friction and the minimum fluidization rate of the bed.

Yu et al. [4] studied the pressure drop in non-Newtonian fluidized beds for Stokes flows and proposed an experimental relationship based on his results to estimate the minimum fluidization velocity. Kawase and Ulbrecht [8] showed that for some non-Newtonian fluids the Richardson-Zaki [11] equation can be used. They also agreed with this equation by using the Christopher and Middleman's [12] method, which is based on pressure drop in non-Newtonian fluidized beds, for laminar flow when using corrected Reynolds number for non-Newtonian fluid. Brea et al. [6] showed that for non-Newtonian fluid flow in the bed with corrected Reynolds numbers greater than

† To whom correspondence should be addressed.
E-mail: mozafari@meybod.ac.ir

40, the bed expansion follows the Richardson-Zaki equation. But, in the corrected Reynolds numbers less than 40, this equation cannot be used for bed expansion.

Machač et al. [13], by studying the expansion behavior of non-Newtonian solid-fluid fluidized beds, showed that the Richardson-Zaki relation is not valid for creeping flow. They proposed a relation for the expansion of a two-phase non-Newtonian bed in creeping flow in regard to their experimental data. Moreover, Lali et al. [3] studied the drag coefficient in an experimental study for non-Newtonian fluid flow in the fluidized bed and reached an agreement for standard drag numbers of a Newtonian fluid with a corrected Reynolds number of more than one. They studied the wall impact coefficient and showed that for the corrected Reynolds numbers in the range 1 to 200, the relation of the wall impact factor to the Newtonian fluidized bed can be used for the non-Newtonian fluidized bed.

Research on non-Newtonian solid-fluid fluidized beds was generally experimental that despite being accurate and valid, they have some disadvantages such as high cost of experimental modeling and studying as well as limitations in studying flow properties. Thus, proper numerical modeling of such beds along with empirical studies can lead to the rapid development of the knowledge of design and fabrication of these beds that have proven applications in the industry.

Mehrabi et al. [2] utilized the combination of the lattice Boltzmann and the smoothed profile methods to numerically simulate the fluid-solid Newtonian fluidized beds. They reached an agreement with the Ergun-Orning equation [14] by comparing their modeling results for the minimum fluidization velocity rate with the Richardson-Zaki equation for the porosity and bed height. In another study, Mehrabi et al. [15] used this hybrid method for modeling and studying the hydrodynamic behavior of an inverse fluid-solid bed with Newtonian fluid and reached a good agreement with the experimental results. They claimed this method is effective in modeling liquid-solid fluidized beds according to their studies. They suggested using this combination for modeling two-phase fluidized beds.

In this paper, the numerical model presented by Mehrabi et al. [2] for simulating liquid-solid fluidized bed was rewritten for non-Newtonian fluid, and by using its result, the effect of geometric parameters and the operating fluid on the expansion behavior of the bed was studied. Programming was done with Fortran.

2. Geometry and Boundary Conditions

Fluidized beds in industrial applications generally have a vertical cylinder shape filled by solid particles where fluid flow direction is upward from the bottom of the cylinder. Thus, modeling was conducted for a rectangular geometry (2D) with solid particles for flow entering from the bottom of the bed. Fig. 1 shows a schematic of the bed and its geometrical parameters. To study the expansion behavior of the bed and the effect of fluid and parameters that change it, various geometries with multiple operating fluids were investigated. More information about geometries and operating fluids is presented in Tables 1 and 2, respectively. Also, in Table 2, the number of fluid domain divisions are provided; as can be seen, each square millimeter of fluid domain is divided into 10×10 square lattice, which is fine enough to capture the flow behavior. Thus, one unit of length in the LBM units is equal to 0.1 millimeter.

In this study, the numerical method proposed by Mehrabi et al. [2] was utilized to model a two-phase fluid bed in which the boundary condition for left and right walls and interface of the fluid and solid is

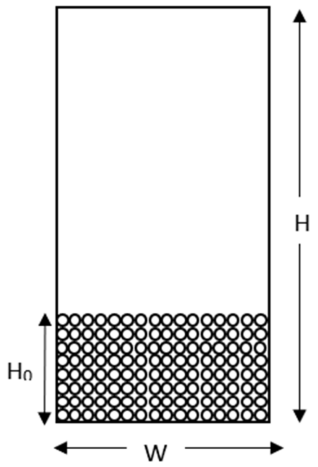

Fig. 1. Schematic geometry of the modeled fluidized bed.

Table 1. Studied fluids specifications

Fluid name	Fluid Density (Kg/m^3)	Viscosity	
		n	k ($Pa.s^n$)
Water	1000	1	0.001
75% Glycerol (Commercial Grade)	1030	1	0.008
CMC 0.1% Solution	1020	0.92	0.008
0.35% Polyox – 301 water solution	1000	0.81	0.0089

Table 2. Specifications of the studied bed geometries

Geometry number	Bed dimensions (mm^2)	Bed dimensions (LBM Unit)	Number of solid particles	The diameter of solid particles (mm)	Initial bed height (mm)
1	20×60	200×600	416	0.6	7.8
2	20×60	200×600	408	0.8	13.6
3	20×60	200×600	423	0.4	3.6
4	15×60	150×600	408	0.6	10.2
5	25×60	250×600	400	0.6	6.0
6	20×60	200×600	240	0.8	8.0
7	20×60	200×600	416	0.4, 0.6, 0.8	10.4

no-slip condition. At the top and bottom walls are assumed to be uniform flow and constant pressure boundary conditions, which is treated by using the Zou and He method in LBM method.

3. Modeling Method

Mehrabi et al. [2] suggested hybrid use of lattice Boltzmann and the smoothed profile methods for numerical modeling of the Newtonian liquid-solid fluidized bed. Their hydrodynamic model is based on the lattice Boltzmann method with the Bhatnagar-Gross-Krook impact function, which its Boltzmann distribution function is in form of Eq. 1.

$$f_\alpha(\vec{X}+\vec{c}_\alpha\delta t.t+\delta t) = f_\alpha(\vec{X}.t)-\frac{1}{\tau}[f_\alpha(\vec{X}.t)-f_\alpha^{eq}(\vec{X}.t)] \quad (1)$$

where $f_\alpha.\delta t.\vec{c}_\alpha.\vec{X}$, and τ are Boltzmann distribution functions for particles, time step, discrete velocity vectors, grid points coordination, and non-dimensional relaxation time, respectively. Bhatnagar-Gross-Krook. f_α^{eq} is the equilibrium distribution function inthe. Batengar-Gruss-Krook impact function that is discretized according to the selected model for velocity in the Boltzmann grid [2]. D_2Q_9 velocity model, which has 9 velocity components based on Eq. 2, is used in this study:

$$\vec{c}_\alpha = \begin{cases} (0.0) & \alpha = 0 \\ \cos(\alpha-1)\frac{\pi}{2}\cdot\sin(\alpha-1)\frac{\pi}{2} & \alpha = 1-4 \\ \sqrt{2}\left(\cos(2\alpha-9)\frac{\pi}{2}\cdot\sin(2\alpha-9)\frac{\pi}{4}\right) & \alpha = 1-4 \end{cases} \quad (2)$$

where α represents the investigated direction. According to the selected velocity model, the equilibrium distribution function is discretized as Eq. 3 [2]:

$$f_\alpha^{eq}(\vec{X}.t) = w_\alpha\rho\left[1+\frac{3u_\alpha}{\vec{c}_\alpha^2}+\frac{9u_\alpha^2}{2\vec{c}_\alpha^4}-\frac{3(\vec{u},\vec{u})}{2\vec{c}_\alpha^2}\right] \quad (3)$$

where u_α is scalar velocity amount in $\vec{c}_\alpha$ direction, ρ is fluid density in Boltzmann grid, and w_α is weight function.

The smoothed profile method is utilized to satisfy the no-slip condition in the interface of solid-liquid and calculating the hydrodynamic forces between solid and fluid particles. This method imposes a bulk force on virtual fluid nodes inside solid particles by adding a term to the collision equation. This force results from the difference between the momentum of the fluid and the solid particle and enforces the virtual fluid nodes to satisfy rigid body motion. In this method, the surface of the solid particle is introduced not as a zero-thickness surface, but as a boundary with a comparable thickness to the unit of grid. Thus, the smoothed profile method shows each solid particle with a smooth curve, called the solid body position curve, that has a value of one in the solid region, zero in the fluid region, and changes continually from one to zero at the solid-fluid interface. Finally, the Boltzmann distribution function is combined with the smoothed profile method for Newtonian fluid as Eq.4 [2]:

$$f_\alpha(\vec{X}+\vec{c}_\alpha\delta t.t+\delta t) = f_\alpha(\vec{X}.t)-\frac{1}{\tau}[f_\alpha(\vec{X}.t)-f_\alpha^{eq}(\vec{X}.t)]+\frac{3w_\alpha\Delta t}{c_\alpha^2}(\vec{f}_H\cdot\vec{c}_\alpha) \quad (4)$$

where $\vec{f}_H$ is the volume force imposed on the virtual fluid nodes located within the solid particle. Note that in this modeling of linear and angular motion of solid particles is modeled using Newton's law of motion.

In the Boltzmann grid method, the difference between the Newtonian and non-Newtonian fluid equations is that the relaxation time is not constant. Since for non-Newtonian fluids, the apparent viscosity is a function of the shear rate and consequently, in the numerical solution, it is a function of the location of the node and time. Therefore, it is necessary to obtain the relaxation time as a function of time and location. For non-Newtonian power-law fluids, the apparent viscosity follows Eq. 5:

$$\mu' = k(4I_2)\frac{n-1}{2} \quad (5)$$

where μ′, k, and n are the power-law apparent viscosity of the fluid, the non-Newtonian fluid constant coefficient (the stability constant), and the power-law index, respectively. I_2 is the second inequality of the deflection tensor obtained by using Eqs. 6 and 7 in the Boltzmann grid [16].

$$d_{\alpha\beta} = -\frac{3}{2\tau}\sum_{i=0}^{8}(f_i-f_i^{eq})c_{i\alpha}c_{i\beta} \quad (6)$$

$$I_2 = \sum_{\alpha,\beta=0}^{1} d_{\alpha\beta}d_{\alpha\beta} \quad (7)$$

By calculating I_2 and replacing in Eq.5, the power-law apparent viscosity of the non-Newtonian fluid is obtained at the specified node and time. Finally, the dimensionless relaxation time is calculated by the following equation:

$$\tau(\vec{X}.t) = 0.5+3\left(\frac{\mu'(\vec{X}.t)}{\rho}\right) \quad (8)$$

where ρ is the fluid density in the Boltzmann grid. By substituting the dimensionless time obtained from Eq. 8 in Eq. 4, the distribution function equations in the Boltzmann grid method and the smoothed profile for the power-law non-Newtonian fluid is obtained as Eq. 9.

$$f_\alpha(\vec{X}+\vec{c}_\alpha\delta t.t+\delta t) = f_\alpha(\vec{X}.t)-\frac{1}{\tau(\vec{X}.t)}[f_\alpha(\vec{X}.t)-f_\alpha^{eq}(\vec{X}.t)] + \frac{3w_\alpha\Delta t}{c_\alpha^2}(\vec{f}_H\cdot\vec{c}_\alpha) \quad (9)$$

4. Model Validation

In this section, to evaluate the performed modeling, the numerical results have been investigated utilizing the researchers' experimental equations for the minimum fluidization velocity, porosity, and height.

4-1. Minimum fluidization velocity

The presented experimental equations to predict the minimum fluidization velocity in the bed with the Newtonian and non-Newtonian fluids are generally in the form of Eq. 10.

$$Ar = f_1(n.\varepsilon_{mf})Re_{mf}^{n/(2-n)} + f_2(n.\varepsilon_{mf})Re_{mf}^{2/(2-n)} \tag{10}$$

where ε_{mf} is the initial porosity of the bed. Re_{mf} and Ar are minimum fluidization Reynolds and Archimedes number, respectively, which are defined in form of Eqs. 11 and 12, respectively.

$$Re_{mf} = \frac{D_p^n u_{mf}^{2-n} \rho f}{k} \tag{11}$$

$$Ar = \frac{3}{4} C_{D_{mf}} Re_{mf}^{2/(2-n)} \tag{12}$$

where u_{mf}, ρ_f, D_p, and C_D are the minimum fluidization velocity, fluid density, solid particle diameter, and drag coefficient, respectively. Moreover, the mf subscript refers to the time that the bed fluidization process starts.

The functions f_1 and f_2 for the empirical equation of Yu et al. [4] in the bed with non-Newtonian fluid and the experimental equation concluded by Mehrabi et al. [2] of the Organ equation [14] for the bed with Newtonian fluid are presented in Table 3. Chhabra et al. [17] reported a 20 to 25 percent mean error for Yu's experimental equation [4] to estimate the minimum fluidization velocity.

Results of bed modeling for three working fluids from Table 1 and geometry from Table 2, along with calculated values from experimental equations for minimum fluidization velocity of the Newtonian and non-Newtonian fluidized bed are presented in Table 4 for comparison and evaluation.

According to Table 4, the results of the model show a good agreement with Mehrabi et al.'s equation [2] for the Newtonian fluidized bed. For the non-Newtonian fluidized bed by considering the reported mean error for the Yu's experimental equation [4] and comparing it with the results in Table 4, output results can also be estimated as acceptable for the non-Newtonian fluidized bed.

Table 3. f_1 and f_2 forms of experimental equations for Newtonian and non-Newtonian fluids

Researcher	f_1	f_2	Fluid
Mehrabi et al. [2]	$150\frac{(1-\varepsilon)^2}{\varepsilon^3}$	$1.75\frac{1}{\varepsilon^3}$	Newtonian
Yu et al. [4]	$\frac{12.5}{\varepsilon_{mf}^{2n+1}}\left[\frac{(9n+1)(1-\varepsilon_{mf})}{n}\right]^n$	0	Non-newtonian

4-2. Porosity and bed height

The model results for porosity and height have also been evaluated and validated with the experimental results, which for the Newtonian fluidized bed, the Richardson-Zaki's experimental equation [11] (Eq. 13) and for the non-Newtonian fluidized bed, the Machač et al.'s experimental equation [13] (Eq. 14) is used.

$$\frac{u}{u_T} = \varepsilon^z \tag{13a}$$

$$\frac{4.8-z}{z-2.4} = 0.043 Ar^{0.57}\left[1-2.4\left(\frac{D_p}{D_b}\right)^{0.27}\right] \tag{13b}$$

where D_b is the fluidized bed diameter and U_T is the terminal velocity.

$$\frac{u}{u_T} = \frac{s}{s_{max}} \tag{14a}$$

$$\varepsilon_{max} = \left\{1 + 0.73(1-n) - 0.79\left(\frac{D_p}{D_b}\right)\right\}^{-1} \tag{14b}$$

$$Z = 6.3 + 7(1-n) - 15.6(D_p/D_b) \tag{14c}$$

To calculate the terminal velocity for replacing in the Eq. 14a, it is necessary to calculate the drag coefficient for the non-Newtonian fluid. In this study, the approximation presented by Lali et al. [3] is used to calculate the drag coefficient in the non-Newtonian fluidized beds.

The results for mean porosity and mean height of the bed obtained from the modeling of the bed with geometry 1, along with the results of the Richardson-Zaki experimental equation for water in Fig. 2a, the experimental equation of Machač et al. [13] for 0.1% CMC solution in Fig. 2b and the 0.35% Polyox-301 solution in Fig. 2c are presented for comparison as a function of the entering fluid velocity to the bed.

According to Fig. 2, simulation results at superficial velocities near the minimum fluidization velocity obtain lower values for porosity and bed height. As apparent fluid velocity increases, the difference between the results decreases, and at higher velocities, model results show higher porosity and bed height than experimental results. Overall, model outputs for the Newtonian and non-Newtonian fluidized beds are in good agreement with the experimental results.

5. Expansion Behavior of the Bed

5-1. Bed fluidization and expansion process

Figure 3 shows the process of fluidization of the bed with geometry 1, particle density of 2500 kg/m^3, and 0.1% CMC solution as working

Table 4. Comparison of minimum fluidization velocity from simulation results with those estimated by experimental correlations

Fluid	Minimum fluidization velocity(m/s)			Error (%)
	Mehrabi et al. [2]	Yu et al. [4]	Model result	
Water	0.00119	-	0.00127	6.7
0.1% CMC solution	-	0.00096	0.0011	14.5
0.35% Polyox – 301 water solution	-	0.00141	0.00115	18.4

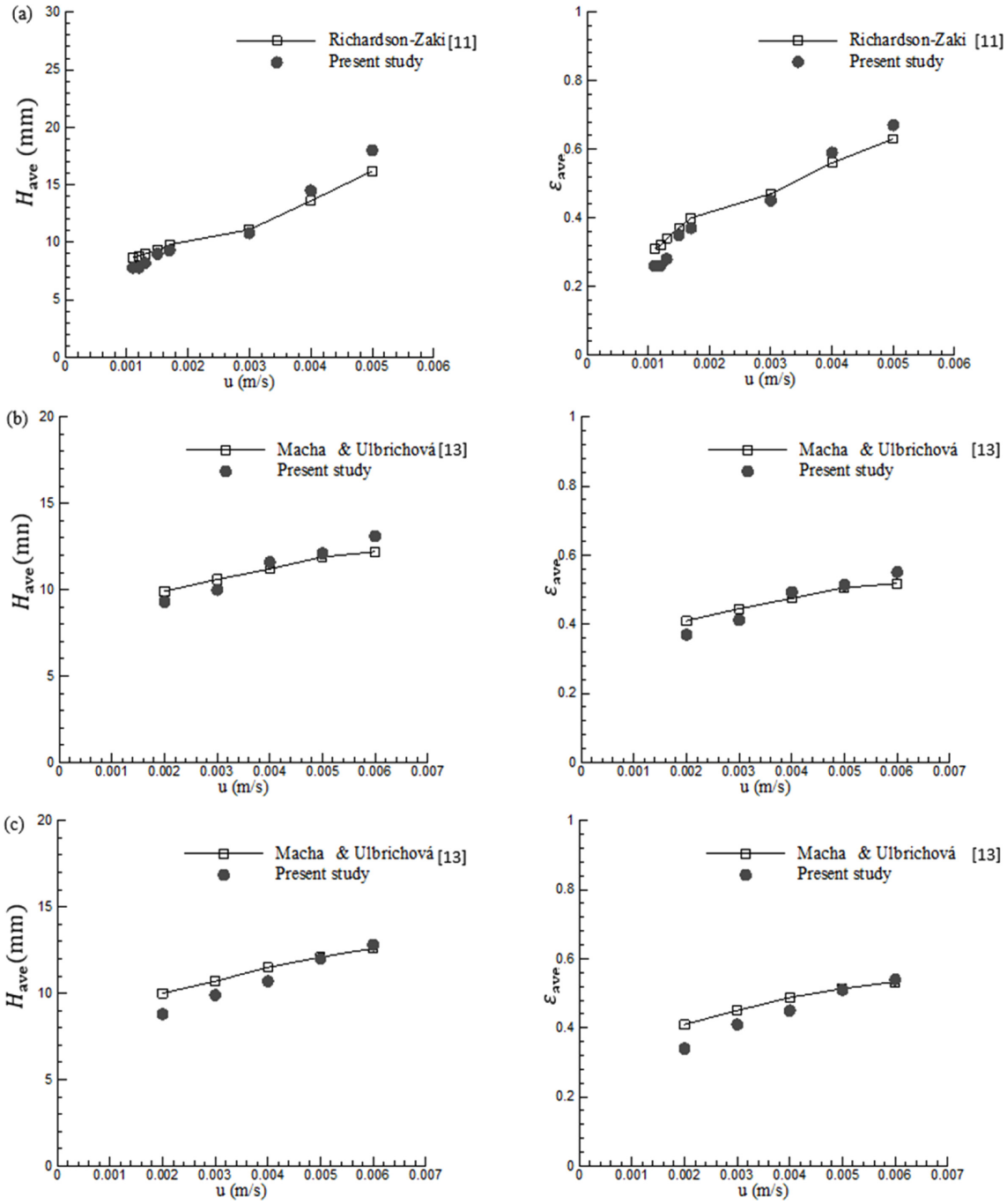

Fig. 2. Comparison of average bed height (left one) and average bed porosity (right one) as a function of the imposed superficial liquid velocity from the simulation with those predicted by the experimental equation for bed geometry 1 and particle density of 2500 kg/m^3 with a) Water, b) 0.1% CMC, c) 0.35% Polyox – 301 water solution.Fig. 9. Bed images for geometry 2 (up ones) and 6 (down ones), particle density of 2500 kg/m^3 and 0.1% CMC as working fluid with inlet velocity of 0.005 m/s in 4 different times as: a) 1 s, b) 2 s, c) 3 s and d) 4 s.

fluid at a superficial velocity of 0.005 m/s for four different times. The bed is in the initial steps in Fig. 3a and the bed particles are in their initial arrangement. After 2.2 seconds the particles are expanded in the middle of the bed and its height increases; however, the particles near the wall retained their original state due to the wall effects (Fig. 3b). Figure 3c shows the bed at 2.7 seconds. At this moment the bed has completely lost its original shape and the overall shape of the bed is unstable. In the end, the bed reaches its final height and steady state after 9 seconds. At this time and afterward, particles move permanently from one side to the other and the general shape of the bed is retained (Fig. 3d).

5-2. Effect of the fluid change on the expansion behavior of the bed

To investigate the effect of the fluid change on the expansion behavior, for the bed with geometry 1, particle density of 2500 kg/m^3

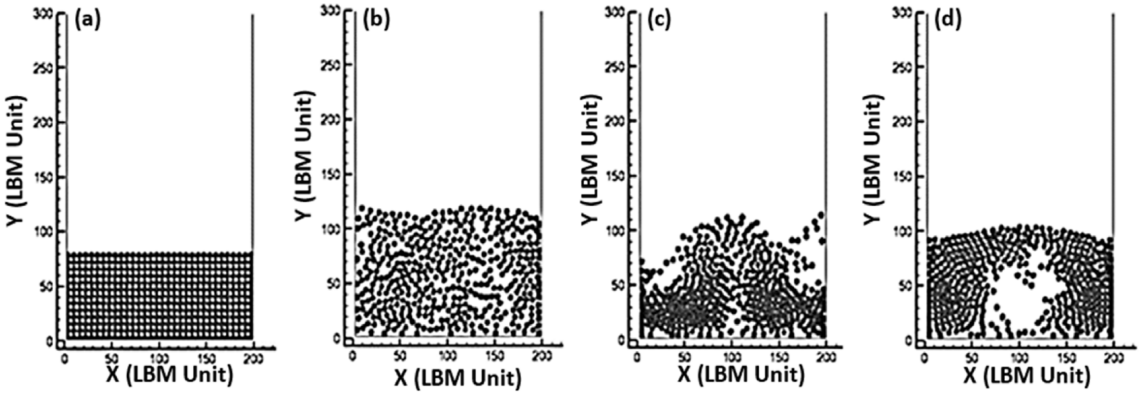

Fig. 3. The process of fluidization of the bed with geometry 1, particle density of 2500 kg/m^3 and 0.1% CMC solution as working fluid at the superficial velocity of 0.005 m/s for four different times: a) initial, b) 2.2s, c) 2.7s and d) 9s.

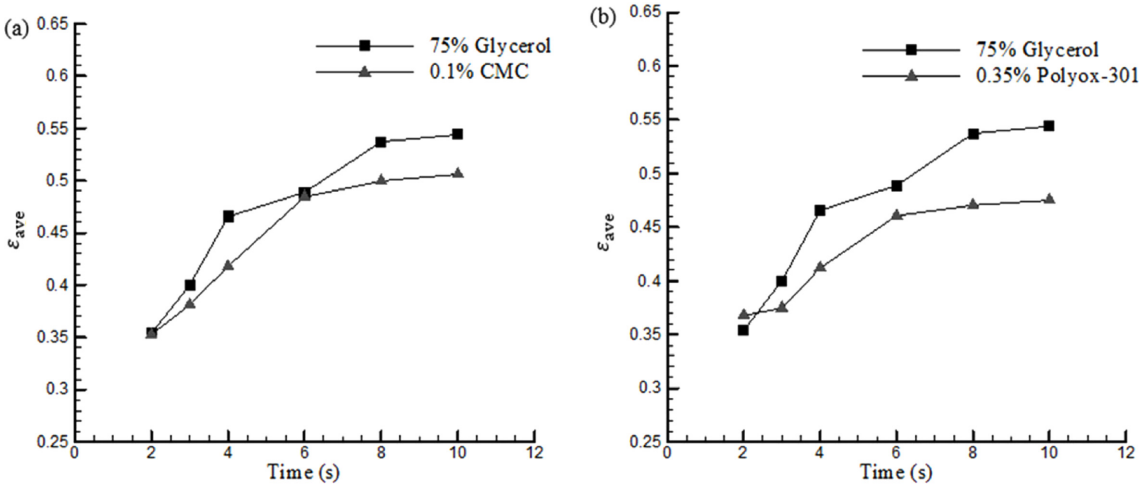

Fig. 4. Average bed porosity as a function of time for bed with geometry 1 and two different fluid (Newtonian and non-Newtonian) with 0.005 m/s velocity.

and two Newtonian and non-Newtonian working fluids with a superficial velocity of 0.005 m/s, bed porosity is plotted as a function of time in Fig. 4.

It can be concluded from Fig. 4a that the bed porosity increases with enhancing the index of power-law, since the 0.1% CMC solution and the 75% glycerol solution have equal stability constants (Table 1), and on the other hand, comparing Fig. 4a and 4b confirms this conclusion. Moreover, considering the slope of the porosity versus time diagram for the bed with the polyox-301 solution and comparing it with the other two curves, it is clear that increasing the fluid stability constant decreases the rate of increase of the porosity over time in the bed.

In Fig. 4b, and at a time of 2 seconds, the porosity of the bed with non-Newtonian fluid is larger than the one with Newtonian fluid. It should be noticed that the height reported in Fig. 4b is the average bed height, and the reason for its greater amount at second 2 is the extreme instability in the shape of the bed, which is a result of more severe effects of the wall on the non-Newtonian fluid bed compared to that of the Newtonian fluid.

5-3. Effects of particles diameter on bed expansion behavior

For the bed with geometries 2 and 3 in Table 2, particle density of 2500 kg/m^3 and 0.1% CMC solution as working fluid with inlet

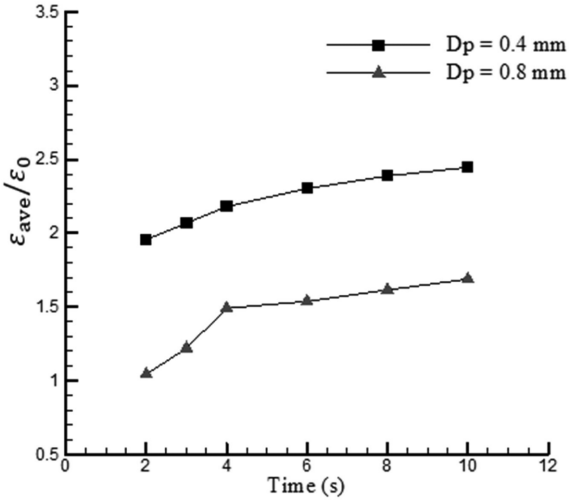

Fig. 5. Variation of bed porosity ratio as a function of time for geometry 2 and 3 with 0.1% CMC as the working fluid and particle density of 2500 kg/m^3.

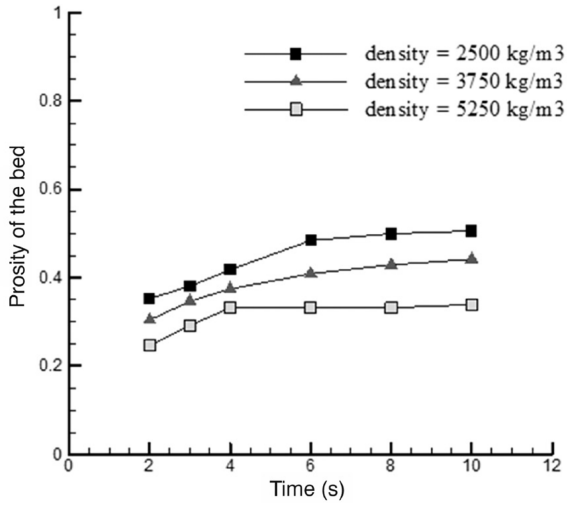

Fig. 6. Bed porosity with geometry 1 and 0.1% CMC solution with an inlet velocity of 0.005 m/s for the three densities of 2500 kg/m^3, 3750 kg/m^3 and 5250 kg/m^3.

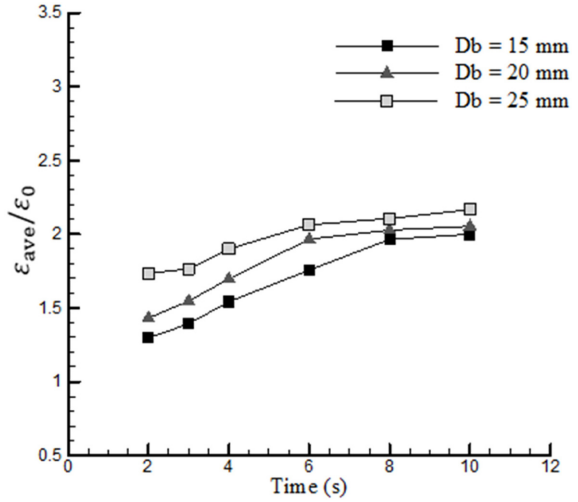

Fig. 7. Bed porosity ratio as a function of time for geometry 1, 4 and 5, particle density of 2500 kg/m^3 and 0.1% CMC with inlet velocity of 0.005 m/s.

velocity 0f 0.005m/s, bed porosity ratio versus time is plotted in Fig. 5. According to this figure, by doubling particle diameter, the bed porosity ratio is decreased by an average of 50% during the process, reaching 88% in the initial moments of the fluidization process. Moreover, by doubling the diameter of the particles until the second 4, according to the slope of the curves, increasing the porosity rate is enhanced due to the increase in initial bed height.

5-4. Effects of particles density on the bed expansion behavior

Another parameter that has been investigated in this study is the effect of the density of solid particles on the expansion behavior of fluidized bed. Figure 6 shows the bed porosity with geometry 1 and 0.1% CMC solution with an inlet velocity of 0.005 m/s for the three densities of 2500 kg/m^3, 3750 kg/m^{3,} and 5250 kg/m^3 as a function of time.

According to Fig. 6, by increasing particle density the average porosity decreases, because the particle's weight force is increased by increasing density; however, the drag force on the solid particles is constant. Moreover, concerning the curves in Fig. 6, by increasing the density of the solid particles, the bed reaches its steady state in a shorter time.

5-5. Effects of bed diameter on expansion behavior

To investigate the effect of bed diameter on expansion behavior, geometries 1, 4, and 5 from Table 2, particle density of 2500 kg/m^3 and 0.1% CMC solution with an inlet velocity of 0.005 m/s are modeled and the porosity ratio for these three beds is plotted as a function of time.

According to Fig. 7, by increasing the diameter of the fluidized bed, the bed porosity ratio increases due to the decrease in wall effects. A comparison of geometries 1 and 5 with 0.1% CMC solution, shows that the 160% increase in bed diameter has increased the porosity ratio by an average of 20%. Moreover, by comparing the results in Figures 5 and 7, it can be concluded that the effect of decreasing the diameter of solid particles for increasing the porosity ratio in the bed is two-times greater than the effect of increasing the bed diameter for this purpose. This conclusion can be used in the design and optimization of non-Newtonian fluidized beds.

5-6. Effect of initial bed height on expansion behavior

To investigate the effect of initial bed height on porosity ratio, geometries 2 and 6 were modeled with 0.1% CMC solution with an inlet velocity of 0.005 m/s, particle density of 2500 kg/m^3 and the results of porosity ratio as a function of time for two beds is presented in Fig. 8.

According to Fig. 8, the porosity ratio decreases by increasing the initial bed height. Moreover, by comparing the slope of the curves up to the second 4, it can be understood that the bed porosity ratio

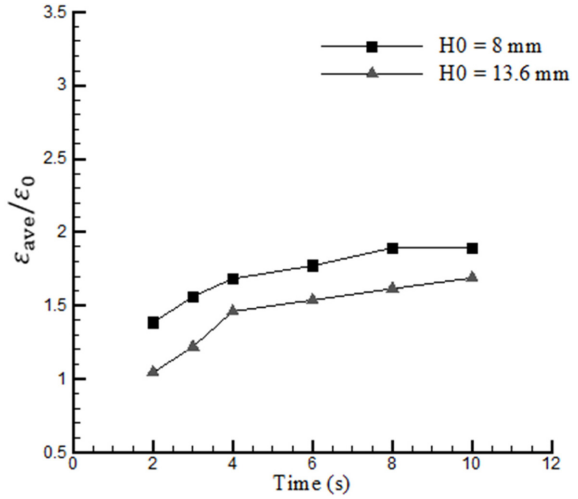

Fig. 8. Bed porosity ratio as a function of time for geometry 2 and 6, particle density of 2500 kg/m^3 and 0.1% CMC as bed fluid with an initial velocity of 0.005 m/.

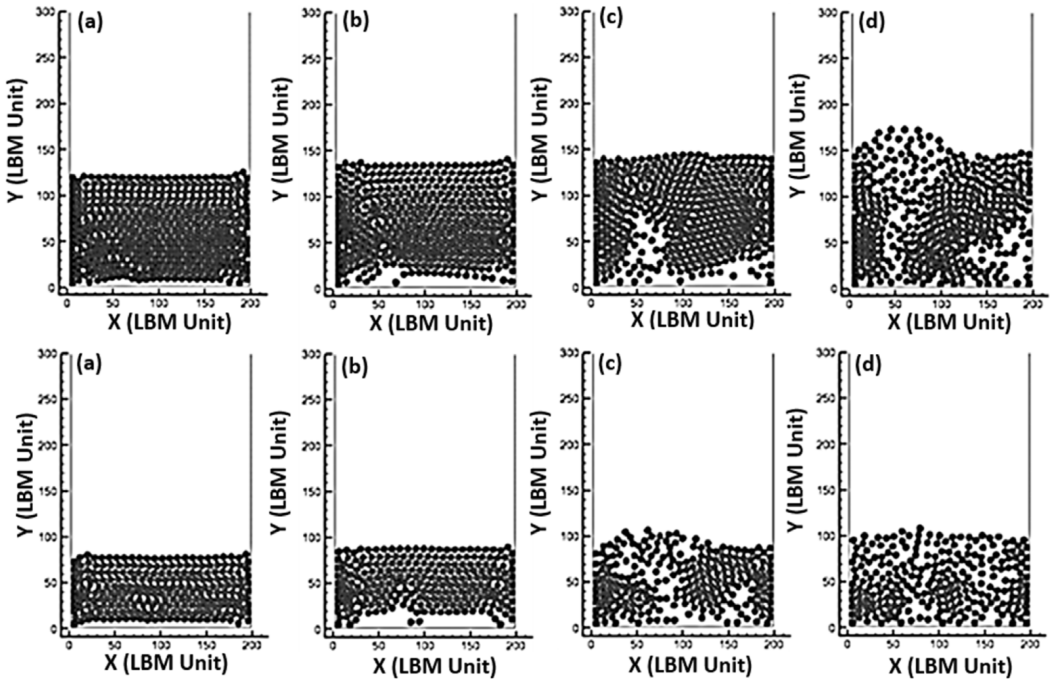

Fig. 9. Bed images for geometry 2 (up ones) and 6 (down ones), particle density of 2500 kg/m^3 and 0.1% CMC as working fluid with inlet velocity of 0.005 m/s in 4 different times as: a) 1 s, b) 2 s, c) 3 s and d) 4 s.

increase rate, increases by the increase of the initial bed height at the initial moments of the fluidization process. The reason for this phenomenon is maintaining the initial arrangement of the particles in the bed with a higher height in initial moments.

In the initial moments of the fluidization process, by entering the working fluid and due to the wall effects, expansion starts from the middle of the bed and particles rise there. However, particles near the wall maintain their initial arrangement and stay at their position. Thus, extreme middle expansion leads to a quicker increase of the porosity ratio in bed that maintains a longer time by increasing the initial height of the bed. Figure 9 shows the initial 4 seconds of the fluidization process in two modeled beds in this section.

According to Fig. 9, the bed with an initial higher height (geometry 2) could maintain the arrangement of particles in walls up to the second 4; however, the bed with lower height (geometry 6) lost its initial arrangement in the second 3.

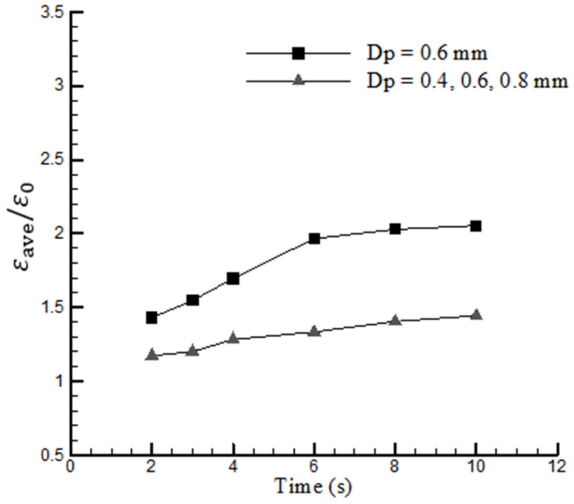

Fig. 10. Bed porosity ratio as a function of time for geometry 1 and 7, particle density of 2500 kg/m^3 and 0.1% CMC as bed fluid with inlet velocity of 0.005 m/s.

5-7. Effects of coexistence of particles with different diameters on the expansion behavior

In industrial applications, all particles in the bed do not have the same diameter. Moreover, in some applications, solid particles in the bed collide with each other or with the wall and transform into smaller particles. Figure 10 shows the porosity ratio as a function of the bedtime for geometries 1 and 7, particle density of 2500 kg/m^3 and 0.1 CMC solution for different times. It should be noticed that in geometry 7, particles with different diameters are entering in a way that the average particle diameter in the bed is equal to the diameter of the ones in geometry 6 (0.6 mm); therefore, the only different parameter between geometries 1 and 7 is the coexistence of particles with different diameter.

According to Fig. 10, the coexistence of particles with different diameter decreases the porosity ratio in the bed by an average of 25%; therefore, coexistence of particles with different diameters is not generally desired in fluidized beds, since one of the aims is using such beds to increase porosity ratio in industrial applications.

Figure 11 shows the fluidization process in the bed with geometry 7 for four different times. According to this figure, during the process of fluidization, particles of lower diameter move down the bed, and

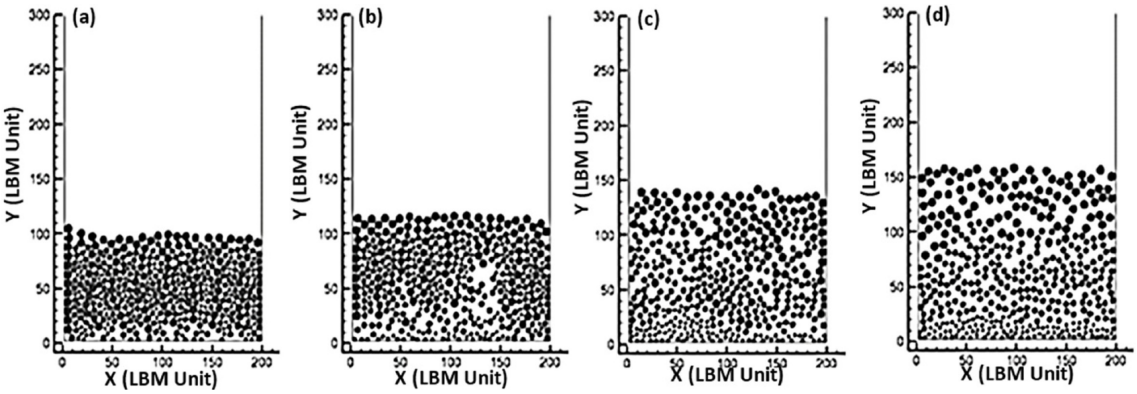

Fig. 11. Fluidization procedure for bed with geometry 7, particle density of 2500 kg/m^3 and 0.1% CMC with an inlet velocity of 0.005 m/s for four different times as a) 1 s, b) 2 s, c) 6 s and d) 26 s.

particles of higher diameter move up the bed and, after separating, their movement is limited to a specific height and level (Fig. 11d). Therefore, if solid particles of a different diameter are present in the bed, eventually, at the steady state of the bed, these particles are separated from each other and place at a certain height. This state is desired in some applications such as separation processes; however, in applications such as heat transfer, constant particle diameter causes the particle to move throughout the bed and according to Fig. 10, it provides 25% more porosity, which is certainly more desired for enhancing the heat transfer than the state of coexistence of particles with different diameters.

6. Conclusion

A liquid-solid two-phase fluidized bed with non-Newtonian fluid was modeled by combining the Boltzmann grid and smoothed profile methods. To study the effect of the change of working fluid and geometric parameters on expansion behavior and porosity of the bed, several different geometries with three different working fluids were studied in this research. Results show that, in general, the bed with Newtonian fluid provides a higher porosity ratio than the non-Newtonian fluid with a power-law index lower than one. Increasing the power-law index leads to a porosity increase in the fluidized bed.

Investigations for solid particle diameter showed that the porosity ratio in the bed is inversely correlated with the solid particle diameter change. A double increase in particle diameter caused a 50% decrease in the bed porosity ratio while the working fluid was 0.1% CMC solution. Increasing solid particle density and initial bed height also reduced the bed porosity. Model outputs for bed with different diameters illustrated that increasing the bed diameter leads to an increase of the fluid bed porosity ratio. Comparisons for changing bed diameter and solid particle diameter showed that the effect of reducing particle diameter on the increase of the bed porosity ratio is two-times greater than the effect of increasing fluidized bed diameter for this purpose. Also, results showed that the porosity ratio in the bed with solid particles of equal diameters is higher than of the particles with different diameters. For 0.1% CMC solution with equal solid particle diameter, the average porosity ratio during the process was 25 percent more than the state with three different diameters for solid particles. Besides, the study of the fluidization process in the beds with different particle diameters showed that during the process, particles are sorted based on their diameters along the bed and each group of them is limited to a specific height of the bed.

References

1. Weber, E., *Crown Ethers.* Ullmann's Encyclopedia of Industrial Chemistry, 2000.
2. Mehrabi Gohari, E., et al., "Hydrodynamic Simulation of a Liquid–solid Fluidized Bed Using Lattice Boltzmann and Smoothed Profile Methods," *Asia-Pacific J. Chemical Engineering*, **12**(2), 196-211(2017).
3. Lali, A., et al., "Behaviour of Solid Particles in Viscous Non-newtonian Solutions: Settling Velocity, Wall Effects and Bed Expansion in Solid-liquid Fluidized Beds," *Powder Technology*, **57**(1), 39-50(1989).
4. Yu, Y., C. Wen, and R. Bailie, "Power-law Fluids Flow Through Multiparticle System," *The Canadian Journal of Chemical Engineering*, **46**(3), 149-154(1968).
5. Mishra, P., Singh, D. and Mishra, I., "Momentum Transfer to Newtonian and Non-newtonian Fluids Flowing Through Packed and Fluidized Beds," *Chemical Engineering Science*, **30**(4), 397-405(1975).
6. Brea, F., Edwards, M. and Wilkinson, W., "The Flow of Non-newtonian Slurries Through Fixed and Fluidised Beds," *Chemical Engineering Science*, **31**(5), 329-336(1976).
7. Kumar, S. and Upadhyay, S., "Mass and Momentum Transfer to Newtonian and Non-newtonian Fluids in Fixed and Fluidized Beds," *Industrial & Engineering Chemistry Fundamentals*, **20**(3), 186-195(1981).
8. Kawase, Y. and Ulbrecht, J., "Mass and Momentum Transfer with Non-newtonian Fluids in Fluidized Beds," *Chemical Engineering Communications*, **32**(1-5), 263-288(1985).
9. Benedict, R. F., Kumaresan, G. and Velan, M., "Bed Expansion and Pressure Drop Studies in a Liquid-solid Inverse Fluidised

Bed Reactor," *Bioprocess Engineering*, **19**(2), 137-142(1998).
10. Lakshmi, A. V., et al., "Minimum Fluidization Velocity and Friction Factor in a Liquid-solid Inverse Fluidized Bed Reactor," *Bioprocess Engineering*, **22**(5), 461-466(2000).
11. Richardson, J. and Zaki, W., "This Week's Citation Classic," *Trans. Inst. Chem. Eng.*, **32**, 35-53(1954).
12. Christopher, R. H. and Middleman, S., "Power-law Flow Through a Packed Tube," *Industrial & Engineering Chemistry Fundamentals*, **4**(4), 422-426(1965).
13. Machač, I., Ulbrichova, I., Elson, T. P. and Cheesman, D. J., "Fall of Spherical Particles Through Non-newtonian Suspensions," *Chemical Engineering Science*, **50**(20), 3323-3327(1995).
14. Ergun, S. and Orning, A. A., "Fluid Flow Through Randomly Packed Columns and Fluidized Beds," *Industrial & Engineering Chemistry*, **41**(6), 1179-1184(1949).
15. Mehrabi Gohari, E., Sefid, M. and Jahanshahi Javaran, E., "Numerical Simulation of the Hydrodynamics of An Inverse Liquid–solid Fluidized Bed Using Combined Lattice Boltzmann and Smoothed Profile Methods," *Journal of Dispersion Science and Technology*, **38**(10), 1471-1482(2017).
16. Boyd, J., Buick, J. and Green, S., "A Second-order Accurate Lattice Boltzmann Non-newtonian Flow Model," *Journal of Physics A: Mathematical and General*, **39**(46), 14241(2006).
17. Chhabra, R. P., Comiti, J. and Machač, I., "Flow of Non-newtonian Fluids in Fixed and Fluidised Beds," *Chemical Engineering Science*, **56**(1), 1-27(2001).

Authors

Mohsen Mozafari-Shamsi: Assistant professor of Mechanical Engineering at Meybod University, Meybod, Yazd, Iran; Mozafari@meybod.ac.ir

Alireza Malooze: Master's student of Mechanical Engineering at Yazd University, Yazd, Iran; ml_alireza72@yahoo.com

Mohammad Sefid: Master's degree in mechanical engineering at Yazd University, Yazd, Iran; mhsefid@yazd.ac.ir

Mostafa Soroor: Master's degree in mechanical engineering at Tarbiat Modares University, Tehran, Iran; m.soroor@modares.ac.ir

Ehsan Mehrabi Gohari: Assistant professor of Mechanical Engineering at Payam-e-Noor University, Tehran, Iran; mehrai.ehsan@gmail.com